JOURNAL OF MATERIALS SCIENCE **35** (2000) 5111–5119

Hydration of Nafion® studied by AFM and X-ray scattering

P. J. JAMES, J. A. ELLIOTT*, T. J. McMASTER
University of Bristol, H.H. Wills Physics Laboratory, Tyndall Avenue, Bristol, BS8 1TL, UK

J. M. NEWTON, A. M. S. ELLIOTT
National Power Innogy, Harwell International Business Centre, Harwell, Didcot, OX11 0QA, UK

S. HANNA‡, M. J. MILES
University of Bristol, H.H. Wills Physics Laboratory, Tyndall Avenue, Bristol, BS8 1TL, UK
E-mail: s.hanna@bristol.ac.uk

Nafion® is a commercially available perfluorosulphonate cation exchange membrane commonly used as a perm-selective separator in chlor-alkali electrolysers and as the electrolyte in solid polymer fuel cells. This usage arises because of its high mechanical, thermal and chemical stability coupled with its high conductivity and ionic selectivity, which depend strongly on the water content. The membrane was therefore studied in different states of hydration with two complementary techniques: atomic force microscopy (AFM) and small angle X-ray scattering (SAXS) combined with a maximum entropy (MaxEnt) reconstruction. Tapping mode phase imaging was successfully used to identify the hydrophobic and hydrophilic regions of Nafion. The images support the MaxEnt interpretation of a cluster model of ionic aggregation, with spacings between individual clusters ranging from 3 to 5 nm, aggregating to form cluster agglomerates with sizes from 5 to 30 nm. Both techniques indicate that the number density of ionic clusters changes as a function of water content, and this explains why the bulk volumetric swelling in water is observed to be significantly less than the swelling inferred from scattering measurements.

1. Introduction

Nafion® is a commercially available perfluorosulphonate cation exchange membrane (CEM) manufactured by E I du Pont de Nemours & Co. Inc. It is commonly used as a permselective separator in chlor-alkali electrolysers [1, 2] and as the electrolyte in solid polymer fuel cells (SPFC). Perfluorosulphonate cation exchange membranes are used in these applications because of their high ionic conductivity and their high mechanical, thermal and chemical stability. Structurally, Nafion consists of a hydrophobic tetrafluoroethylene (TFE) backbone with pendant side chains of perfluorinated vinyl ethers terminated by ion-exchange groups. The chemical structure of Nafion is shown in Fig. 1. The ion content can be varied by changing the ratio of the two components.

Other perfluorosulphonate cation exchange membranes with similar structures have also been developed by the Asahi Chemical Company (Aciplex®) and the Asahi Glass Company (Flemion®). The Dow Chemical Company also developed a material with a shorter side-chain than those of Nafion and the other perfluorosulphonates [3].

The ionic conductivity in perfluorosulphonate membranes is important since it should be as high as possible to minimize ohmic losses in chlor-alkali electrolysers and to maintain high output power densities in fuel cell applications. The membrane conductivity is strongly influenced by the water content [4]. Water management is also an important problem for efficient SPFC operation to avoid flooding of the gas diffusion electrodes. A number of factors affect the water content including the cation form, ion exchange capacity of the membrane and equivalent weight (EW). The ion content is usually expressed in terms of the equivalent weight of the polymer. The equivalent weight is defined as the weight of dry polymer in grams containing one mole of exchange sites. The desired equivalent weight is achieved by varying the ratio of vinyl ether monomer to TFE. The useful range of equivalent weights is from 600–1500 g per mole, between the solubility and percolation limits. The industrial applications of Nafion have

* *Present Address*: Department of Materials Science and Metallurgy, University of Cambridge, Pembroke Street, CB2 3QZ, UK.
‡ Author to whom all correspondence should be addressed.

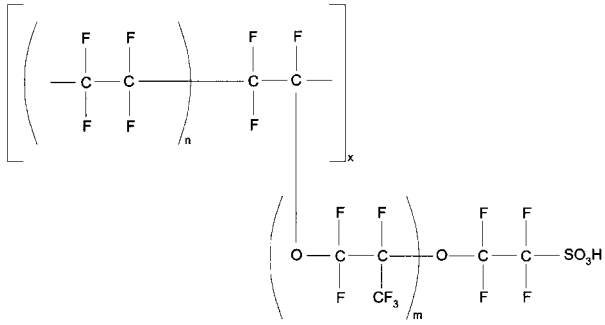

$$C_{(2n+3m+4)}F_{(4n+6m+7)}O_{(m+4)}SH$$

Figure 1 The structural repeat of Nafion.

prompted considerable research effort summarised by Eisenberg and Yeager in 1982 [5] and more recently by Tant *et al*. in 1997 [3].

Perfluorosulphonate polymers typically have ordered structures in which the hydrophilic end groups aggregate within a hydrophobic matrix composed of the fluorocarbon backbone of the polymer. The density contrast between the ionic aggregates and the matrix gives rise to scattering of X-rays [6–9] and neutrons [5]. The diffraction patterns show a broad ring reflection, the so-called 'cluster' reflection, with a peak position of 3.5–5.5 nm, together with a scattering upturn at low angles. Many different structural models have been proposed to explain these features, and they can be divided into two main groups. The first type are the interparticle models, such as the two-phase model [5, 10] and the lamellar model [5, 11], in which the scattering is produced by the interference between ionic aggregates. The second are the intraparticle models, such as the core-shell model [5, 12, 13], in which the scattering is due to fine structure within an individual ionic aggregate.

There have been a number of electron microscopy studies of Nafion [14, 15] which support the cluster model of phase separation, although the size scale of the structures observed did not correspond directly with those detected by scattering studies. The Cluster-Network model [5, 16] postulates a large scale organisation of clusters with transient connective tubes which are in constant flux. A fully-reversible dynamic reorganisation of the clusters is proposed to occur on rehydration. Positron annihilation spectroscopy has also been used to study different cation forms of Nafion membranes by measuring the free volume. These studies [17–19] found that the formation and expansion of clusters is always associated with a change in free-volume structure resulting in smaller free-volume holes.

There have been two recent studies undertaken using scanning probe microscopy (SPM) [20, 21], to investigate the structure of Nafion in differing states of hydration. A number of swelling studies have been carried out on Nafion [22, 23] using a wide variety of solvents with some remarkable results, including a swelling of 360% with tributylphosphate (TBP) as used by Lehmani *et al*. in their SPM study [21]. Nafion has proved to be a suitable sample for other forms of SPM including scanning tunnelling microscopy (STM) and scanning electrochemical microscopy (SECM) [24, 25]. Fan and Bard [24] studied a spin-coated Nafion film using SECM and found a domain-like structure, consisting of circular structures, 1–2 nm in diameter made up from a conductive central zone surrounded by a less conductive region.

Since many of the useful properties of Nafion membranes depend strongly on the water content, studies in different states of hydration using the two complementary techniques of atomic force microscopy (AFM) and small angle X-ray scattering (SAXS), might be informative. The difference in probe-specimen adhesion between the hydrophobic backbone and hydrophilic side group regions of Nafion offers the possibility of observing the spatial distribution of these two regions at the surface of the polymer using tapping mode phase imaging. Assuming that these are representative of the bulk, then the number density and average cluster size can be deduced as a function of water content, and the results compared with those from SAXS experiments.

2. Experimental method

2.1. Variation of the mass of Nafion with humidity

The uptake of water in Nafion membranes has been studied as a function of environmental humidity using a dynamic vapour sorption study (DVS) [26]. The sample was suspended in a 0% RH environment and weighed. The humidity was increased in steps using different saturated salt solutions, the sample was allowed to equilibrate and then weighed, the process was then repeated. A graph of percentage mass gain versus humidity was plotted from the data. Given that the equivalent weight of the sample and the theoretical weight are known, the average number of water molecules per sulphonic acid group can be calculated at 0% RH, by comparing the theoretical weight to the measured value. If it is assumed that all of the water is incorporated into the hydrophilic regions, a graph of average number of water molecules per sulphonic acid group can be plotted over the full range of humidities.

2.2. Sample preparation

All of the experiments were carried out using the most commonly used form of Nafion, $115H^+$, which has the following physical properties; a nominal equivalent weight of 1100 (actually 1070) and thickness of 5 thousandths of an inch ($\sim$127 μm).

The membrane will readily rehydrate if left exposed to a high relative humidity environment [27]. Careless handling can result in the membrane ion-exchanging from the acid (H^+) to a salt form (e.g. Na^+ or K^+). All samples were therefore routinely prepared by refluxing with a 50/50 mixture by volume of concentrated nitric acid and de-ionized water, then de-ionized water alone, to ensure that the membrane is in the H^+ form and free from any chemical impurities.

2.3. Small-angle X-ray scattering

Two dimensional, point collimated SAXS data were collected using nickel-filtered Cu K_α radiation on a flat plate Rigaku-Denki camera, with a typical sample to

film distance of around 250 mm. The X-ray generator was an Elliott GX21 rotating anode generator. The films were scanned in transmission using an Optronics P2000 drum densitometer. The resulting images were converted to 8-bit binary files, with a pixel dimension of 100×100 μm. The low-angle limit due to beam divergence was approximately 0.026 nm^{-1}, which corresponds to a maximum discernible size for features in real space of around 40 nm. The diffraction patterns were corrected for Lorentz-polarisation effects and sample absorption.

Previous studies of SAXS from hydrated ionomer membranes used heat-sealed polymer bags to enclose the samples during exposure [6, 7]. This method was found to be unsatisfactory for quantitative work due to fluctuations in the environmental humidity level during the long periods (up to 24 hours) required to collect the SAXS data. An alternative approach, based on the controlled humidification of air using concentrated salt solutions, was adopted [28].

2.4. Maximum entropy method

A full account of the maximum entropy (MaxEnt) method used to interpret SAXS data has already been published [29], and only a summary will be presented here. The aim of the MaxEnt technique is to reconstruct a two dimensional charge density map which is a good fit to the observed scattering data. The MaxEnt criterion is required in order to resolve the inherent ambiguity in this fitting process due to the absence of phase information in the experimental data. Since there are many charge distributions which can give rise to identical diffraction patterns, we select the one with the highest entropy for a given goodness-of-fit. Of course, there is no guarantee that this model will necessarily be stereochemically or thermodynamically realistic, but if a reasonable structural interpretation can be found then we can be sure that this it is the most statistically likely interpretation which is consistent with the scattering data. In this way, the MaxEnt method is superior to other approaches which assume *a priori* a structural model. The algorithm used to carry out the reconstruction process is based on the 'Cambridge Algorithm' [30].

2.5. Atomic force microscopy

There are two principal modes of atomic force microscopy (AFM) [31] operation: contact mode and tapping mode. In contact mode, the tip remains in close contact with the sample, operating within the repulsive regime. In tapping mode, the cantilever is oscillated near to its resonant frequency, above the surface, only contacting the surface briefly during each cycle of its oscillation. Tapping mode is therefore more suitable for imaging delicate samples owing to the lower lateral forces and has been applied to many polymer systems [32–35]. It also has the added advantage of being able to obtain phase images as well as topographical data. Tapping mode phase imaging is a relatively new AFM technique, and it can differentiate between areas with different properties regardless of their topographical nature [36–42]. The phase angle is defined as the phase lag of the cantilever oscillation relative to the signal sent to the piezo driving the cantilever. Its value depends on the energy dissipated in the tapping interaction of probe and specimen [43, 44].

Circular samples 10 mm in diameter were mounted on magnetic stainless steel stubs, placed in the Digital Instruments Extended Multimode AFM and imaged in tapping mode with silicon cantilevers in order to provide topographic and corresponding phase images. The membrane and microscope were placed in a purpose-built environmental chamber to control the humidity and the samples were dehydrated overnight. A variety of techniques was employed to reduce the humidity including silica gel, phosphorus pentoxide, a liquid nitrogen cold finger and dry nitrogen gas. A humidity minimum of (0.8 ± 2.0)% was obtained using nitrogen gas passed through molecular sieve material. The sample was then imaged and allowed to rehydrate slowly to room humidity (34 ± 2)% over the course of 12 hours whilst being continuously imaged, and the humidity recorded.

2.6. Cluster counting algorithm

Phase images from the beginning and end of the rehydration sequence were analysed with the aid of a cluster counting algorithm [28, 45]. The 256×256 images were exported, cropped, saved as eight-bit data and then converted to binary. A series of thresholds from 0 to 256 was then applied to all the data points in the image; if the point was equal to or greater than the threshold value it was set to one (white), and, if not, it was set to zero (black). A cluster is defined as an isolated group of white pixels. The number of unique clusters, total area of clusters and average cluster area was then calculated for each threshold. The number of clusters at each threshold value was plotted for the two humidity extremes. The same algorithm was also used to analyse the MaxEnt reconstructions of the SAXS data acquired at ambient and 100% relative humidity.

3. Results and discussion

3.1. Variation of the mass of Nafion with humidity

Analysis of the DVS results is more revealing than previous studies [27]. In addition to a graph of percentage mass change against humidity (Fig. 2i), a graph of the ratio of water molecules to sulphonic acid groups against humidity (and not just the additional number) can be plotted (Fig. 2ii). This has been calculated using a theoretical dry mass for Nafion and by assuming that the EW is 1070. The difference in mass between the theoretical dry mass and that at 0% RH is the amount of water bound to the sulphonic acid groups. The average number of water molecules per sulphonic acid group at 0% RH was found to be 1.55. In the same regime as that used for the AFM data, in the humidity range of $(0–50) \pm 2$%, on average an additional water molecule was added to each sulphonic acid group for an increase in RH of 14 ± 2%. At higher humidities this becomes much more rapid and the assumption that all of the water is incorporated into the hydrophilic regions become less valid as water will start to condense on all regions of the membrane.

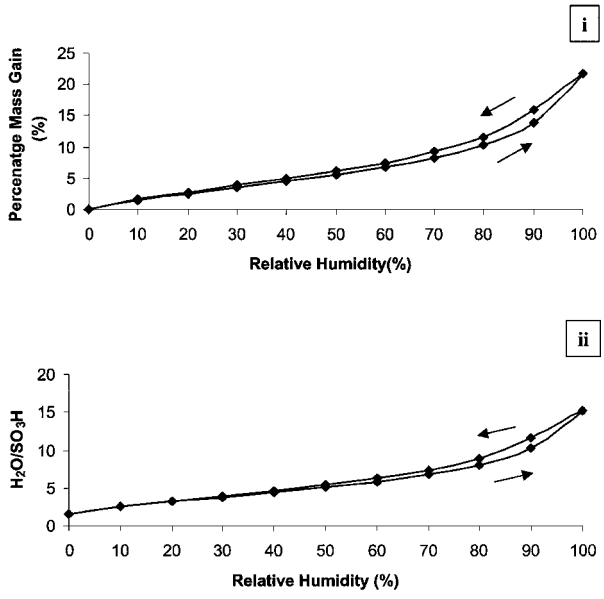

Figure 2 Percentage mass gain (i) and Number of addition water molecules per sulphonic acid group (ii) against relative humidity for Nafion 115 H^+. The relative humidity was cycled from to 0 to 100% and back again.

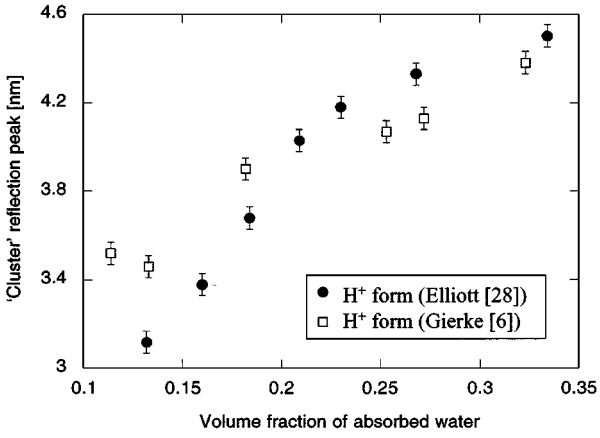

Figure 3 Peak position of the 'cluster' reflection from Nafion 115 H^+ membrane as a function of the volume fraction of absorbed water.

3.2. Small-angle X-ray scattering

The variation in the peak position of the 'cluster' reflection in the SAXS from a Nafion 115 H^+ membrane as a function of the volume fraction of absorbed water is shown in Fig. 3, along with the data published by Gierke *et al.* [6] for comparison. There are no values below a volume fraction of 0.1 as it was not possible to detect the 'cluster' reflection at such low water contents due to lack of electron density contrast. The dependence of the peak position on water content is predicted by the type of scattering model which is used to interpret the data. If the 'cluster' reflection were due to the coherence of intercluster spacings [5, 10], or the incoherent sum of interlamellar spacings [5, 11] then it might be expected that the increase in peak position would be directly proportional to the volume of absorbed water. However, if the reflection were produced by the scattering from individual three dimensional clusters models [5, 12, 13] then its spacing should vary with the cube root of the water volume. In fact, neither of these two simple behaviours occurs.

In order to explain the observed swelling behaviour, it is instructive to consider a MaxEnt interpretation of the scattering data. Fig. 4 shows MaxEnt reconstructions from membranes under ambient and 100% RH conditions. The MaxEnt reconstructions should be interpreted as 2-dimensional projections of the electron density distributions within a representative volume of membrane. Regions of low electron density appear light grey or white, while regions of high electron density appear dark grey or black. The absolute electron density range in each case is scaled to fit the grey-scale. The reconstructions are not unique, belonging to a large set of possible maximum entropy solutions, all of which are capable of reproducing the experimental data subject to the usual errors associated with X-ray counting statistics. However, the region of membrane represented in the reconstructions is sufficiently large that it is able to reproduce a wide range of structural variation within a single electron density map.

Both MaxEnt reconstructions contain fragmented regions of low charge density with a broad range of sizes. There is an increase in electron density contrast between these regions and the background, along with a coarsening of the size distribution from Fig. 4i (ambient) to Fig. 4ii (100% RH). In order to make the physical interpretation of these features clear, the reconstructions were spatially filtered to separate the small scale structures associated with the 'cluster' reflection from the large scale structures associated with the scattering upturn. The filtering was performed by windowing out the unwanted regions of the diffraction patterns, prior to MaxEnt reconstruction. The high spatial frequency images, shown in Fig. 4iii and iv for ambient and 100% RH respectively, both contain collections of point-like scatterers. However, as the water content is increased from Fig. 4iii to Fig 4iv, the spacing between the scatterers increases, and their number density decreases. It is the coherence of the spacings between the scatterers that is responsible for the 'cluster' reflection, and this interpretation is borne out by reconstructions from highly oriented samples [45]. We therefore identify the point-like scatterers as being individual ionic clusters.

The low spatial frequency images, shown in Fig. 4v and vi, show large scale structures which are composed of agglomerates of the clusters identified in the high frequency images. Although the agglomerates do not swell appreciably with increasing water content, the electron density contrast between these features and the polymer matrix increases noticeably due to the difference in density between the water and fluorocarbon phases. The shape of these cluster agglomerates, which is responsible for the form of the low angle upturn in the SAXS pattern, is related to the spatial coherence of the clusters. We therefore predict an intimate relation between the form of the upturn and the degree of arcing of the 'cluster' reflection. If the MaxEnt interpretation of the SAXS data is correct, then it should not be possible to see an arced 'cluster' reflection unless the low angle upturn is also anisotropic.

Assuming the MaxEnt interpretation is correct, then it is useful to calculate the relative number density of ionic clusters in Fig. 4iii and iv and relate this to the discrepancy between the bulk swelling of the membrane

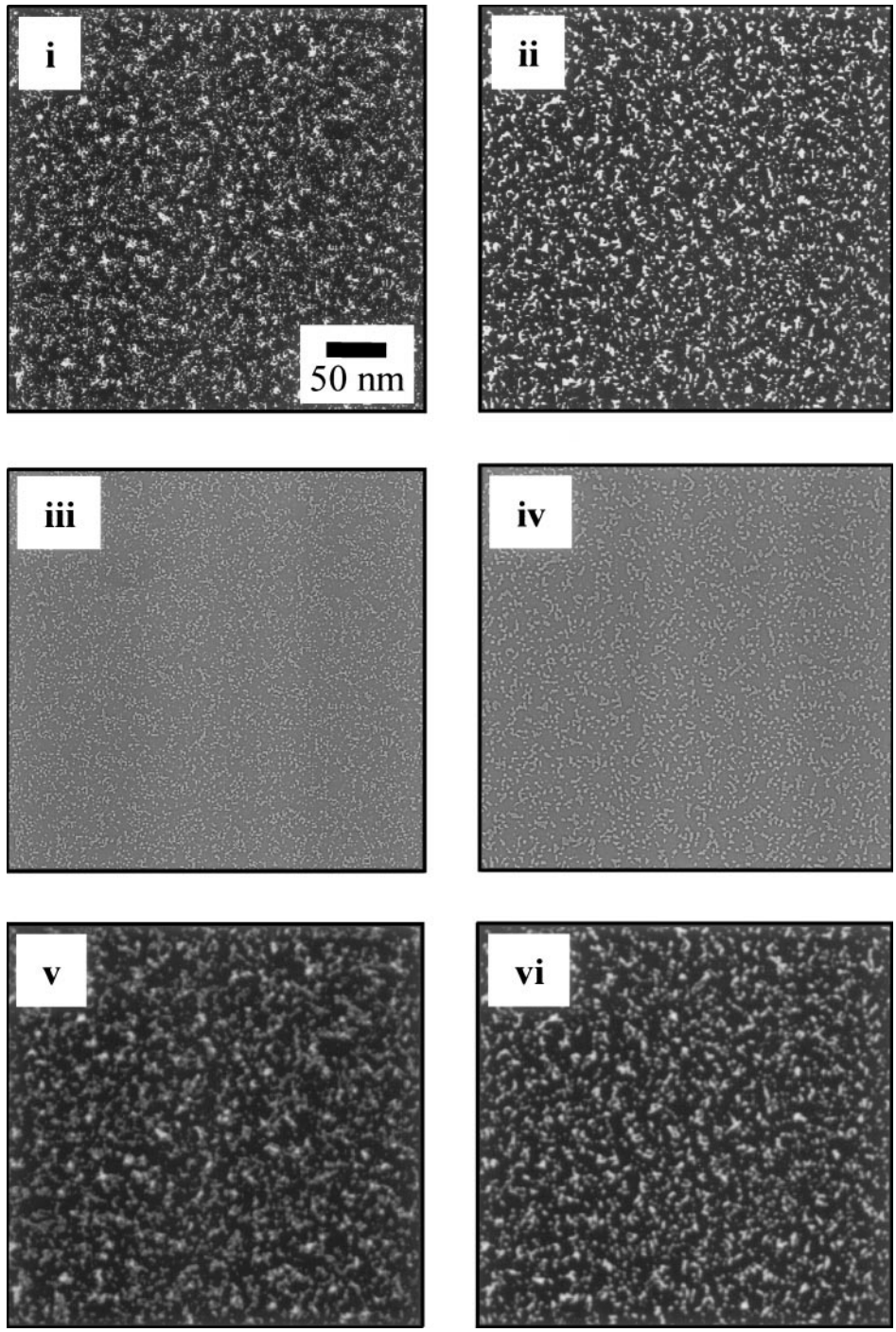

Figure 4 MaxEnt reconstruction of SAXS data from Nafion 115 H^+ membrane: (i) ambient humidity and (ii) 100% RH. The reconstructions have been high pass filtered in (iii) and (iv) and low pass filtered in (v) and (vi).

and the swelling which is inferred from the increase in the peak position of the 'cluster' reflection. Although the mean lateral intercluster separation increased by 44.1%, the overall lateral expansion of the membrane is expected to be significantly less than this due to a decrease in the number density of clusters. Unfortunately, it is difficult to predict the resultant macroscopic swelling quantitatively, because the electron density distributions are a 2-dimensional representation of 3-dimensional space. It is also possible that systematic changes in the spatial ordering of the clusters on swelling need to be incorporated into the model. Nevertheless, the mechanism described is qualitatively appealing and has been derived with the use of only very general *a priori* hypotheses, i.e.: (i) the use of a MaxEnt electron density distribution, (ii) the legitimacy of spatial filtering and (iii) the definition of a 'cluster' as an isolated agglomerate of pixels.

Although the redistribution of exchange groups was first predicted by the Marx infinite paracrystalline model [10] it is significant that this phenomenon can be inferred directly from the small angle X-ray data. In addition, there is also evidence for such a redistribution from phase contrast atomic force microscopy as discussed in the following section.

3.3. Atomic force microscopy

Six 1 μm phase images from a sequence of 56 images of 1070EW Nafion obtained over a range of humidities from (9–34) $\pm$ 2% are shown in Fig. 5i–vi. The phase

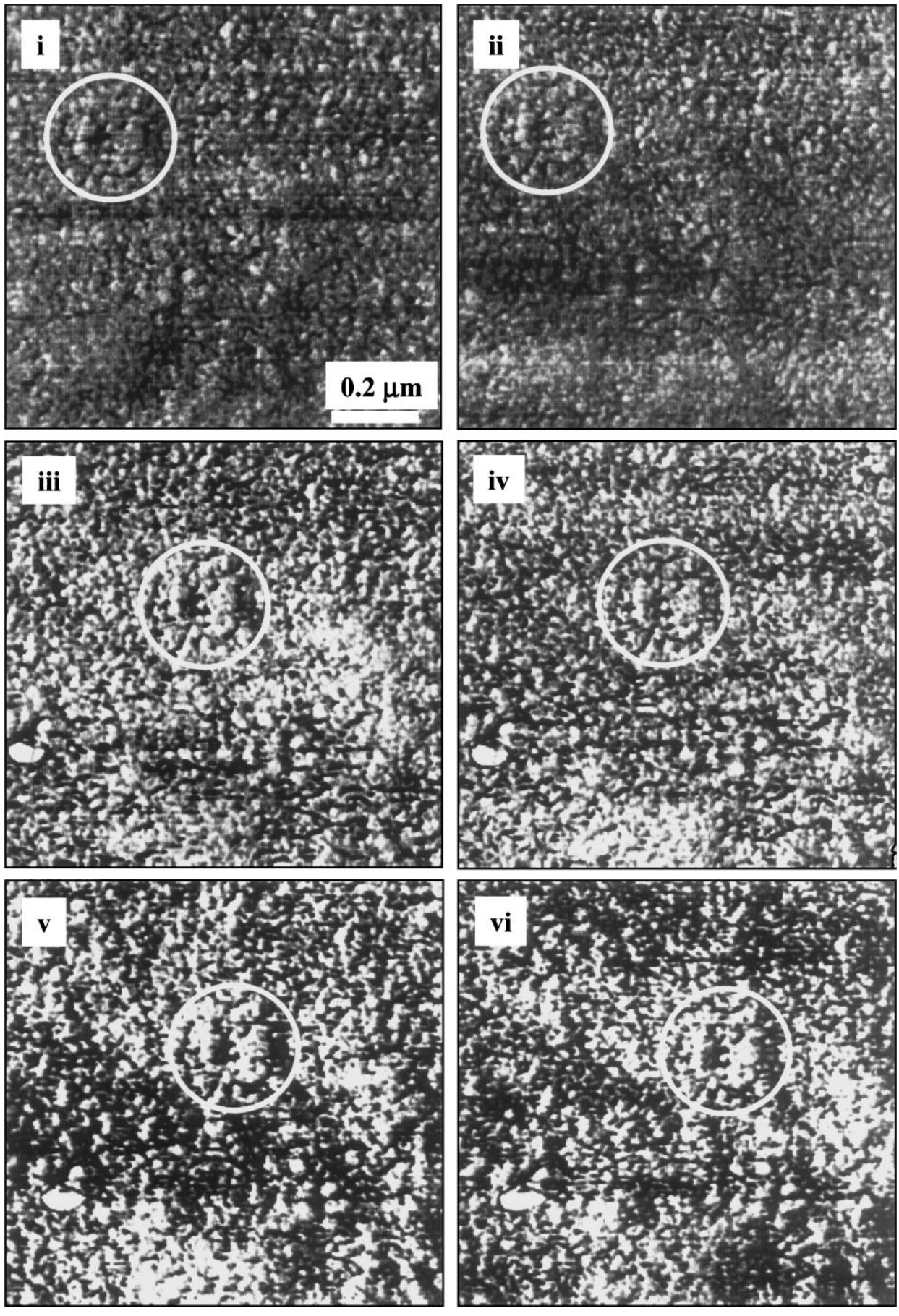

Figure 5 Six 1 μm tapping mode phase images of the same area of Nafion at relative humidities of (i) 9, (ii) 13, (iii) 19, (iv) 23, (v) 28 & (vi) 33 $\pm$ 2% (Z scale = 30°).

contrast between the hydrophilic sulphonic acid groups and the hydrophobic regions increases with humidity due to preferential sorption of water to the hydrophilic regions. It is very difficult to monitor the same area as the membrane expands both vertically and laterally. The same feature has been circled in each of the images to aid comparison and to illustrate the drift to the right which occurred throughout the series.

Cluster-like structures with a diameter of 5–30 nm are clearly visible, particularly in the phase images. These structures do not always correspond to features in the height image. Features at the same height can have a different phase signal and vice versa, indicating minimal topographic coupling. This is consistent with the earlier AFM studies [20, 21]. Chomakova-Haefke *et al*. [20], produced samples by evaporating a dilute solution of Nafion on to gold-sputtered cover slips. They were found to have a fibril network structure, which became more ordered as the membrane swelled. Lehmani *et al*. [21], imaged commercially available nominally 1100 EW Nafion 117. It was dehydrated in a vacuum oven at 80 °C and was first imaged "dry", then swollen with de-ionized water, and finally swollen with TBP. A super-structure of spherical domains with an average diameter of 45 nm containing 11 nm grains was found. According to the section analysis of the microstructure, the interstitial regions have a mean thickness of 5 nm, which may correspond to the cluster size.

The corresponding topography images from the beginning and end of the rehydration sequence are shown in Fig. 6i and ii respectively. The same area has been circled in both images demonstrating the ability to image the same area whilst following a dynamic process. There is no appreciable change between the two images, therefore any topographic coupling in the phase images remains constant and is not responsible for the increase in phase contrast.

Cluster counting analysis of the phase images from the beginning and end of the rehydration sequence is shown in Fig. 7i and ii, respectively, and tabulated in Table I. The sharp peak in Fig. 7i implies that all of the clusters have a similar phase angle and therefore energy loss at lower humidities. At higher humidities as shown in Fig. 7ii, the peak has moved to higher thresholds as the average energy loss has increased; the peak has also broadened significantly as the clusters have a wider range of energy losses. The average cluster area of between 134 and 158 nm^2 is consistent with the images shown in Fig. 5, where clusters have a range of linear dimensions between 5 and 30 nm (or

TABLE I The number of clusters, total percentage area of cluster and average cluster size for 1 μm wide phase images of Nafion at (9 & 34) $\pm$2% relative humidity

Humidity $\pm$2%	9	34
Number of Cluster	1415	1118
Total Percentage Cluster Area	18.9	17.6
Average Cluster Area (nm^2)	134	158

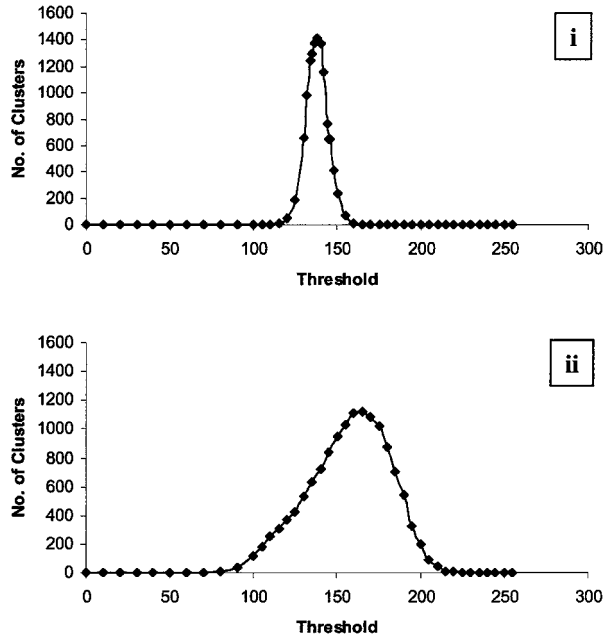

Figure 7 A graph of number of clusters against threshold value for the two humidity extremes of 9 & 34 $\pm$ 2%.

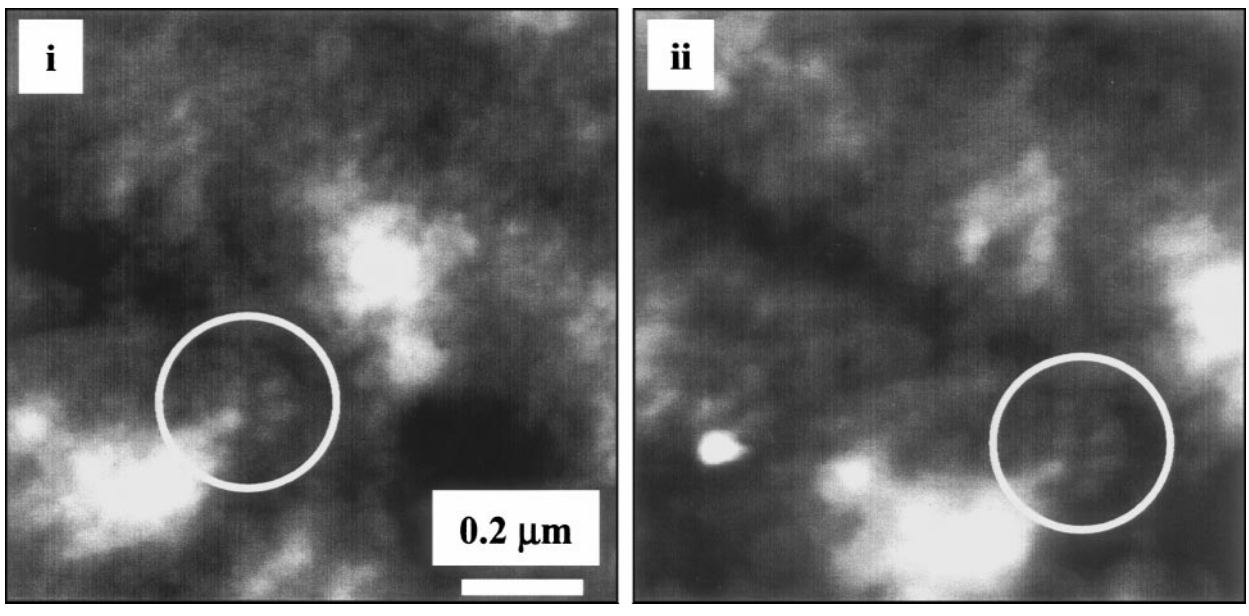

Figure 6 Topography images corresponding to those in Fig. 5i and vi for the humidity extremes of 9 & 34 $\pm$2%. (Z scale = 50 nm).

approximate areas of 25 to 900 nm^2). This is significantly larger than the individual clusters which give rise to the 'cluster' reflection, but of comparable size to the cluster agglomerates.

The decreasing number of clusters and corresponding increase in average cluster size with humidity is consistent with the X-ray diffraction results described in the previous section and implies a cluster rearrangement similar to that proposed by Hsu & Gierke [16]. The percentage of the surface covered by clusters at 34 and 9% humidities, is 17.6 and 18.9% respectively. The larger percentage area at lower humidities can easily be explained by tip broadening effects, whereby a greater number of small features can appear to have disproportionately larger area than fewer larger features. This is considerably larger than a value of 7.6% calculated assuming: that the membrane is homogeneous and dry, that the mass of SO_3H is 81.1 g and the equivalent weight of the membrane to be 1070 (i.e. $(81.1/1070) \times 100$). However, the membrane is not dry and will have incorporated water preferentially into the hydrophilic clusters which will have swollen, the surface may not be representative of the bulk and the sulphonic acid group composition is 8% by mass, but not by volume.

4. Conclusions

The average number of water molecules per sulphonic acid group in Nafion 115 at 0%RH was found to be 1.55. If it is assumed that all of the additional water is incorporated into the hydrophilic regions as the humidity increased then in the approximately linear region between $(0–50) \pm 2\%$ RH an increase of $14 \pm 2\%$ in RH resulted in one additional water molecule per sulphonic acid group.

The most statistically likely structural model compatible with the MaxEnt reconstruction of the small angle X-ray scattering (SAXS) data is an interparticle model in which point-like ionic clusters aggregate to form higher order agglomerates.

Tapping mode phase imaging was successfully used to identify the hydrophobic and hydrophilic regions of Nafion perfluorosulphonate cation exchange membranes. Since there is often little correlation between the topography and phase images, it is a useful tool for identifying and mapping regions with different properties, irrespective of their topographical nature. The images support the MaxEnt interpretion of a cluster model of ionic aggregation, with spacings between individual clusters ranging from 3 to 5 nm, aggregating to form cluster agglomerates with sizes from 5 to 30 nm.

The phase images also showed that the number of clusters decreased and the average cluster size increased with increasing humidity. This is consistent with the interpretation of the MaxEnt charge distributions, and is reminiscent of the redistribution of ionic material between clusters proposed in the cluster-network model [16]. The change in number density of ionic clusters as a function of water content explains why the bulk volumetric swelling in water is observed to be significantly less than the swelling inferred from scattering measurements.

It is significant that the same conclusions were obtained using two different experimental techniques operating over complementary ranges of relative humidity. This indicates that the swelling and redistribution of ionic clusters in Nafion is a dynamic process occurring continuously from 0% to 100% relative humidity.

Acknowledgements

PJ would like to thank Dr. James Wescott for his assistance with the computer programming. This work was financially supported by the EPSRC and National Power Innogy as part of their ongoing research into regenerative fuel cell technology.

References

1. H. L. YEAGER and A. STECK, *Journal of the Electrochemical Society* **128** (1981) 1880.
2. H. L. YEAGER, B. O'DELL and Z. TWARDOWSKI, *ibid.* **129** (1982) 85.
3. M. R. TANT, K. A. MAURITZ and G. L. WILKES, "Ionomers: Synthesis, Structure, Properties and Applications" (Chapman & Hall, London, 1997).
4. T. A. ZAWODZINSKI, T. E. SPRINGER, J. DAVEY, R. JESTEL, C. LOPEZ, J. VALERIO and S. GOTTESFELD, *Journal of the Electrochemical Society* **140**(7) (1993) 1981.
5. A. EISENBERG and H. L. YEAGER, "Perfluorinated Ionomer Membranes" (ACS Books, Washington, 1982).
6. T. D. GIERKE, G. E. MUNN and F. C. WILSON, *Journal of Polymer Science Part B-Polymer Physics* **19**(11) (1981) 1687.
7. E. J. ROCHE, M. PINERI, R. DUPLESSIX and A. M. LEVELUT, *ibid.* **19**(1) (1981) 1.
8. M. FUJIMURA, T. HASHIMOTO and H. KAWAI, *Macromolecules* **14**(5) (1981) 1309.
9. *Idem., ibid.* **15**(1) (1982) 136.
10. C. L. MARX, D. F. CAULFIELD and S. L. COOPER, *ibid.* **6** (1973) 344.
11. E. J. ROCHE, R. S. STEIN, T. P. RUSSELL and W. J. MACKNIGHT, *Journal of Polymer Science Part B-Polymer Physics.* **18** (1980) 1497.
12. W. J. MACKNIGHT, W. P. TAGGART and R. S.STEIN, *Journal of Polymer Science Symposium C* **45** (1974) 113.
13. J. KAO, R. S. STEIN, T. P. RUSSELL, W. J. MACKNIGHT and G. S. CARGILL, *Macromolecules* **7** (1974) 95.
14. S. RIEBERER and K. H. NORIAN, *Ultramicroscopy* **41** (1982) 225.
15. Z. PORAT, J. R. FRYER, M. HUXHAM and I. RUBINSTEIN, *Journal of Physical Chemistry* **99** (1995) 4667.
16. W. Y. HSU and T. D. GIERKE, *Journal of Membrane Science* **13**(3) (1983) 307.
17. H. S. SODAYE, P. K. PUJARI, A. GOSWAMI and S. B. MANOHAR, *Journal of Polymer Science Part B-Polymer Physics* **36**(6) (1998) 983.
18. *Idem., ibid.* **35**(5) (1997) 771.
19. G. DLUBEK, R. BUCHHOLD, C. HUBNER and A. NAKLADAL, *Macromolecules* **32**(7) (1999) 2348.
20. M. CHOMAKOVA-HAEFKE, R. NYFFENEGGER and E. SCHMIDT, *Applied Physics A* **59** (1994) 151.
21. A. LEHMANI, S. DURAND-VIDAL and P. TURQ, *Journal of Applied Polymer Science* **68**(3) (1998) 503.
22. G. H. McCAIN and M. J. COVITCH, *Journal of the Electrochemical Society* **131** (1984) 1350.
23. G. GEBEL, P. ALDEBERT and M. PINERI, *Polymer* **34** (1993) 333.
24. F. F. FAN and A. J. BARD, *Science* **270** (1995) 1849.
25. M. V. MIRKIN, *Analytical Chemistry News and Features A* **68** (1996) 177.
26. A. M. S. ELLIOTT, Unpublished research, 1999.

27. B. DREYFUS, G. GEBEL, P. ALDEBERT, M. PINERI, M. ESCOUBES and M. THOMAS, *Journal De Physique* **51**(12) (1990) 1341.
28. J. A. ELLIOTT, PhD thesis, University of Bristol, 1998.
29. J. A. ELLIOTT and S. HANNA, *Journal of Applied Crystallography* **32** (1999) 1069.
30. J. SKILLING and S. F.GULL, "Maximum Entropy and Bayesian Methods in Inverse Problems," edited by C. R. Smith and W. T. Grandy JR. (Dordrecht: Riedel, 1985) p. 83.
31. G. BINNIG, C. F. QUATE and C. GERBER, *Physics Review Letters* **56** (1986) 930.
32. T. J. MCMASTER, J. K. HOBBS, P. J. BARHAM and M. J. MILES, *Probe Microscopy* **1**(1) (1997) 43.
33. J. K. HOBBS, T. J. MCMASTER, M. J. MILES and P. J. BARHAM, *Polymer* **39**(12) (1998) 2437.
34. B. RATNER and V. V. TSUKRUK, "Scanning Probe Microscopy in Polymers" (ACS Books, Washington, 1998).
35. P. J. JAMES, T. J. MCMASTER, J. M. NEWTON and M. J. MILES, *Polymer* **41**(11) (2000) 4223.
36. K. L. BABCOCK and C. B. PRATER, D.I. Application Note A12, 1995.
37. J. TAMAYO and R. GARCIA, *Langmuir* **12** (1996) 4431.
38. P. LECLERE, R. LAZZARONI, J. L. BREDAS, J. M .YU, P. DUBOIS and R. JEROME, *ibid.* **12** (1996) 4317.
39. A. J. HOWARD, R. R. RYE and J. E. HOUSTON, *Journal of Applied Physics* **79** (1996) 1885.
40. M. H. WHANGBO, S. N. MAGONOV and H. BENGEL, *Probe Microscopy* **1** (1997) 23.
41. J. TAMAYO and R. GARCIA, *Applied Physics Letters* **71** (1997) 2394.
42. R. GARCIA, J. TAMAYO, M. CALLEJA and F. GARCIA, *Applied Physics A-Materials Science & Processing* **66**(Pt1SS) (1998) S309.
43. J. P. CLEVELAND, B. ANCZYKOWSKI, A. E. SCHMID and V. B. ELINGS, *Applied Physics Letters* **72**(20) (1998) 2613.
44. J. TAMAYO and R. GARCIA, *ibid.* **73**(20) (1998) 2926.
45. J. A. ELLIOTT, S. HANNA, A. M. S. ELLIOTT and G. E. COOLEY, *Macromolecules* **33** (2000) 4161.

Received 1 February
and accepted 26 February 2000